6-17-2021

Groundwater level assessment and prediction in the Nebraska Sand Hills using LIDAR-derived lake water level

Nawaraj Shrestha
University of Nebraska - Lincoln, nawaraj.shrestha@huskers.unl.edu

Aaron R. Mittelstet
University of Nebraska-Lincoln, amittelstet2@unl.edu

Aaron R. Young
University of Nebraska-Lincoln, ayoung3@unl.edu

Troy E. Gilmore
University of Nebraska-Lincoln, gilmore@unl.edu

David C. Gosselin
University of Nebraska - Lincoln, dgosselin2@unl.edu

See next page for additional authors

Authors

Nawaraj Shrestha, Aaron R. Mittelstet, Aaron R. Young, Troy E. Gilmore, David C. Gosselin, Yi Qi, and Caner Zeyrek

Groundwater level assessment and prediction in the Nebraska Sand Hills using LIDAR-derived lake water level

Nawaraj Shrestha,[1] Aaron R. Mittelstet,[2] Aaron R. Young,[3] Troy E. Gilmore,[2,3] David C. Gosselin,[1] Yi Qi,[1] and Caner Zeyrek[1]

1 School of Natural Resources, University of Nebraska-Lincoln, Lincoln 68583, NE, USA
2 Biological System Engineering Department, University of Nebraska-Lincoln, Lincoln 68583, NE, USA
3 Conservation and Survey Division, School of Natural Resources, University of Nebraska-Lincoln, Lincoln 68583, NE, USA

Corresponding author — A.R. Mittelstet, *email* amittelstet2@unl.edu

Abstract

The spatial variability of groundwater levels is often inferred from sparsely located hydraulic head observations in wells. The spatial correlation structure derived from sparse observations is associated with uncertainties that spread to estimates at unsampled locations. In areas where surface water represents the nearby groundwater level, remote sensing techniques can estimate and increase the number of hydraulic head measurements. This research uses light detection and ranging (LIDAR) to estimate lake surface water level to characterize the groundwater level in the Nebraska Sand Hills (NSH), an area with few observation wells. The LIDAR derived lake groundwater level accuracy was within 40 cm mean square error (MSE) of the

Published in *Journal of Hydrology* 600 (2021) 126582
doi:10.1016/j.jhydrol.2021.126582

Submitted 11 February 2021; revised 11 June 2021; accepted 15 June 2021; published 17 June 2021.

nearest observation wells. The lake groundwater level estimates were used to predict the groundwater level at unsampled locations using universal kriging (UK) and kriging with an external drift (KED). The results indicate unbiased estimates of groundwater level in the NSH. UK showed the influence of regional trends in groundwater level while KED revealed the local variation present in the groundwater level. A 10-fold cross-validation demonstrated KED with better mean squared error (ME) [−0.003, 0.007], root mean square error (RMSE) [2.39, 4.46], residual prediction deviation (RPD) [1.32, 0.71] and mean squared deviation ratio (MSDR) [1.01, 1.49] than UK. The research highlights that the lake groundwater level provides an accurate and cost-effective approach to measure and monitor the subtle changes in groundwater level in the NSH. This methodology can be applied to other locations where surface water bodies represent the water level of the unconfined aquifer and the results can aid in groundwater management and modeling.

Keywords: Groundwater level, Lake groundwater level, Light detection and ranging (LIDAR), Universal kriging (UK), Kriging with an external drift (KED), Remote sensing, Lake surface area

1. Introduction

An accurate representation of groundwater level in aquifers is important to many problems in hydrologic and numerical model analysis and designs. A large number of observation wells help to characterize and analyze the change and vulnerability of aquifers to natural or anthropogenic factors such as climate change and global warming (Desbarats et al., 2002; Döll et al., 2012; Meixner et al., 2016; Scanlon et al., 2006; Taylor et al., 2013). Groundwater level in aquifers, however, due to large installation and maintenance costs, are often sparsely measured and monitored (Singh et al., 2010; Strassberg et al., 2009). Gaps at unsampled locations are often filled using geostatistics with the available measurements, thus leading to uncertainty in the water level prediction. The associated uncertainty can be reduced using an alternate approach such as satellite altimetry to measure and monitor the groundwater level. Satellite altimetry provides remote estimates of water level at the interface of groundwater and surface interaction and provides an increased number of hydraulic heads that can sufficiently characterize the spatial correlation structure and predict the groundwater level with adequate accuracy.

Satellite altimetry measures the range (distance from the satellite to surface), by computing the travel time of the reflected and received pulse from the satellite antenna. With the use of reference ellipsoid, the relative height of the surface is thus determined (Nielsen et al., 2017). Many studies have used satellite altimetry to estimate water surface elevation (Asadzadeh Jarihani et al., 2013). Satellite laser altimeters such as Ice, Cloud, and land Elevation Satellite-2 (ICESat-2) provides sufficient accuracy (<10 cm) to characterize large water bodies but fails to provide good accuracy of smaller and shallow water due to a larger footprint size and use of green (532 nm) laser frequency that penetrates shallow water (Li et al., 2017; Ryan et al., 2020; Yuan et al., 2020; Zhang et al., 2019). Similarly, synthetic aperture radar (SAR) altimeters, such as CryoSat-2 with footprints of 300 m, provide measurements within 15 cm accuracy for larger lakes or water bodies (Nielsen et al., 2017; Roohi et al., 2021). Airborne altimeters, such as light detection and ranging (LIDAR), estimates lake surface elevation for small as well as large water bodies with accuracy ranging from 3–50 cm (Höfle et al., 2009; Hofton et al., 2000; Hopkinson et al., 2011; Paul et al., 2020; Zhang et al., 2020). While airborne LIDAR provides high accuracy for smaller lakes, the widely available topographic LIDAR data suffers from low backscatter and laser dropouts as the near-infrared wavelengths are highly absorbed by water (Fernandez-Diaz et al., 2014; Milan et al., 2010). The uncertainty associated with low backscatter, however, can be reduced using approaches such as the waterline method. The waterline method uses the boundary between the water surface and landmass, derived from the remotely sensed image, and superimposes them on the elevations relative to mean sea level (Bell et al., 2016; Kang et al., 2017; Qi et al., 2019; Yue and Liu, 2019). The water surface boundary from satellite images is generally delineated using methods such as single-band thresholding, classification, multi-band, subpixel, and hybrid approaches (Bijeesh and Narasimhamurthy, 2020; Du et al., 2012). The accuracy is increased when the original bands are combined with transformed spectral bands such as image color space, principal component analysis, tasseled cap transformation (TCT), and water indices (Balázs et al., 2018; Jiang et al., 2012; Ma et al., 2019; Verpoorter et al., 2012; Zhuang and Chen, 2018). Satellite altimetry, therefore, provides remote estimates of groundwater levels in areas where surface and groundwater interact (Zhang et al., 2017). The increased measurements thereby reduce the uncertainty and better characterizes the spatial variation in the groundwater level using geostatistical methods.

Geostatistics are often used to fill the gaps in areas where field observations are sparse. Geostatistics estimate and define the spatial correlation structure from sampled locations and make predictions at unsampled locations. Stochastic methods such as ordinary kriging, universal kriging (UK), kriging with an external drift (KED), and co-kriging are extensively used to map the spatial and temporal variation of groundwater levels (Adhikary and Dash, 2017; Boezio et al., 2006; Varouchakis and Hristopulos, 2013). Ordinary kriging provides an optimal estimate of the groundwater level given the data follow a multivariate normal distribution with a theoretical variogram (Ahmadi and Sedghamiz, 2007; Goovaerts, 1997; Theodoridou et al., 2017; Varouchakis et al., 2016; Varouchakis and Hristopulos, 2013). Groundwater levels with effects of regional trends are modeled using the UK as the linear drift improves the accuracy of the interpolated heads (Adhikary and Dash, 2017; Ahmed, 2007; Kambhammettu et al., 2011). Although UK provides better estimates of groundwater level, when the observations are sparse and linearly associated with external variables, KED improves the estimation of hydraulic heads (Boezio et al., 2006; Desbarats et al., 2002; Deutsch and Journel, 1992; Rivest et al., 2008). As groundwater is the subdued replica of topography (Condon and Maxwell, 2015; Haitjema and Mitchell-Bruker, 2005) and is widely available, digital elevation models are often used to define the external drift (Desbarats et al., 2002; Goovaerts, 2000). For example, Desbarats et al. (2002) used KED with topography as drift and found that the use of topography provides robust estimates of the water table elevation. While methods such as co-kriging incorporates more than one secondary variable in the covariance structure to explain the groundwater level variation, the difference is not always significant (Ahmadi and Sedghamiz, 2008) and requires inference of direct and cross covariance functions. Co-kriging is also cumbersome and time-consuming when many secondary variables are used (Desbarats et al., 2002). Methods other than geostatistics, such as multiple linear regression and neural networks, are also used to predict the groundwater level. These methods, although provide higher accuracy, require a large number of ancillary data to capture the water level variation in an aquifer. Regardless of the interpolation method, the accuracy depends on the distribution, number, and quality of data from observation wells. The spatial correlation structure derived from a few observations is unable to characterize the spatial variability present in the aquifer, thus leading to higher uncertainties and coarser representation of aquifer water level (Buchanan and Triantafilis, 2009; Li and Heap, 2008).

This research combines airborne altimetry with geostatistics and provides a novel approach to estimate the groundwater level in areas of surface water groundwater interchange. The objective of this research was to map the spatial variability of the groundwater levels estimated from LIDAR-derived lake water level in the Nebraska Sand Hills (NSH). The specific objectives of this research were to i) estimate the feasibility of LIDAR-derived groundwater level from lake water level ii) evaluate UK and KED to characterize the groundwater levels and iii) validate/ compare the interpolated groundwater levels to numerical model predicted hydraulic heads and published water table contours.

2. Methods

2.1. Study area

The NSH has an area of 50,000 km^2 and is the largest grass-stabilized dune field in the western hemisphere with 450 km^2 of shallow lakes and 4500 km^2 of subirrigated meadows (**Fig. 1**) (Ahlbrandt and Fryberger, 1980; Smith, 1965; Gosselin et al., 2000; Sweeney and Loope, 2001). The areas of the lakes range from 0.004 to 12 km^2 with most lake depths averaging less than one meter (Gosselin et al, 2000). **Table 1** shows the proportion of lake sizes used in the study. The majority (76%) of the lakes are smaller than 0.2 km^2. The lakes are denser in the western and northern parts of the NSH and sparse in the south (Fig. 1). The semiarid climate of NSH has temperatures ranging from –40 to 43.3 °C with an average annual temperature of 8.9 °C. The annual average precipitation ranges from 450 mm in the west to 690 mm in the eastern part of NSH (National Climatic Data Center, 2020). Lake hydrology is dependent on precipitation and groundwater as

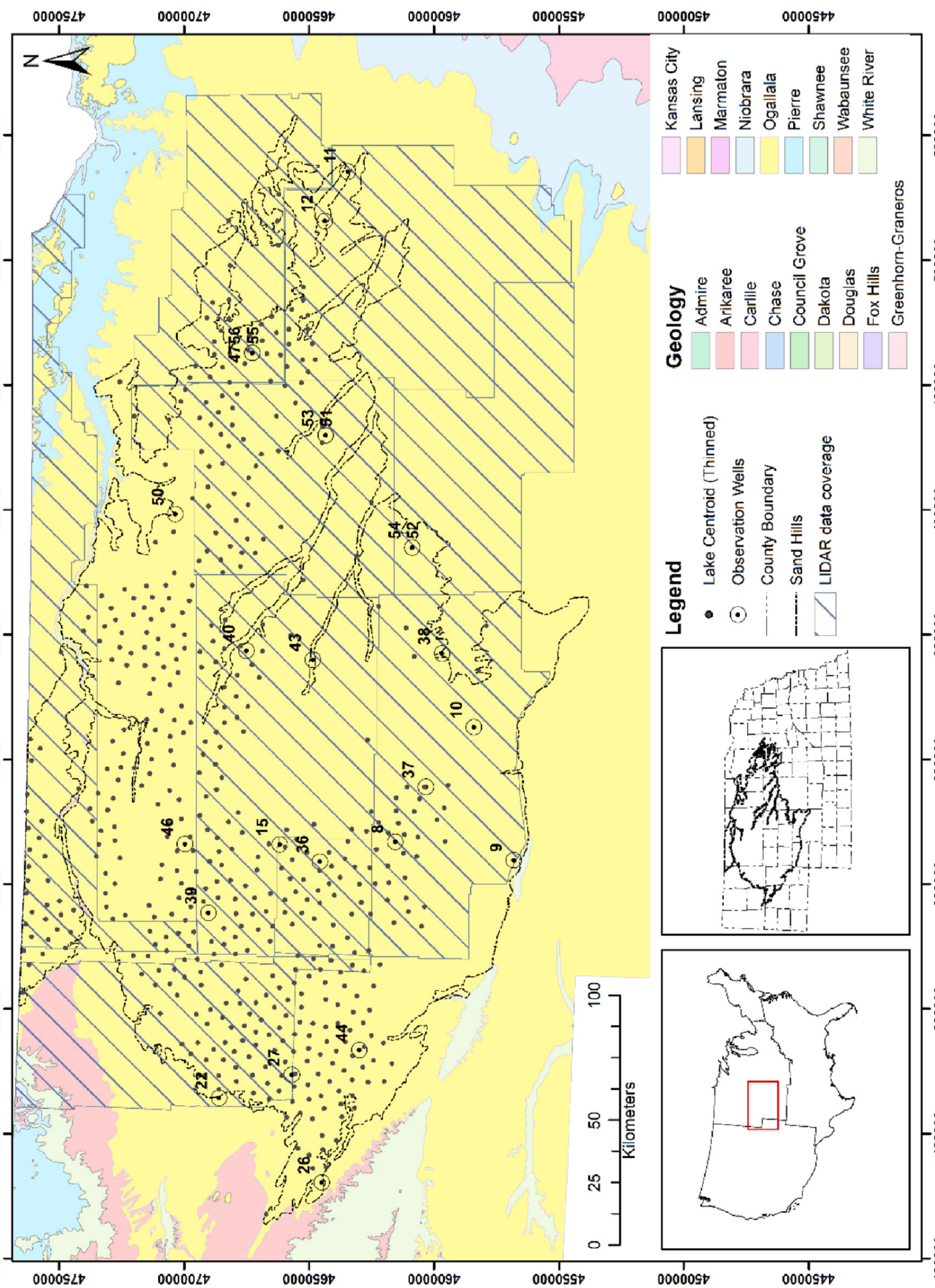

Fig. 1. The Nebraska Sand Hills showing the geology, lakes, observation wells, irrigation wells and LIDAR data coverage. Wells with multiple numbers indicate well nests.

Table 1 Lake size distribution percentage in the study area.

Lake size (km²)	*Percentage*
0–0.2	76.8
0.2–0.5	15.8
0.5–2	6.74
>2	0.717

inputs and evaporation and seepage losses as outputs (Winter, 1986). High total dissolved solid concentrations and water levels lower than the regional potentiometric surface indicate that lakes are focused groundwater discharge areas (Gosselin et al., 2000; Ong, 2010; Winter, 1986; Zlotnik et al., 2009). The evaporation from lakes exceeds the precipitation. For example, the Alkali Lake in the NSH from July to September of 2007–2009 averaged 5.1 mm day^{-1} of evaporation compared to 1.3 mm day^{-1} of precipitation (Riveros- Iregui et al., 2017).

NSH lies on the northern part of the High Plains aquifer system. The Ogallala Group is the dominant and major water bearing geologic unit in the NSH and is formed of moderate to low-permeable sand, sandstone, and siltstones deposited during the mid-Tertiary age (Fig. 1). The aquifer dips gently eastward at 0.9–1.3 m per kilometer (Gutentag et al., 1984) and is part of the High Plains aquifer system, where saturated. In NSH, dunes of the Quaternary age overlie the unconsolidated alluvial sand, gravel, silt, and clay that overlie the Ogallala Group. The dunes, composed of very fine to medium sand, form an important part of aquifer by promoting aquifer recharge (Gutentag et al., 1984; Peterson et al., 2020). The Arikaree Formation and the White River Group, which lie beneath the Ogallala Group, are also part of the High Plains aquifer, though are finer-grained, and only contain usable quantities of water locally at fractured or coarse-grained area. In the western NSH, the Arikaree Group is underlain by the Brule Formation. This unit is composed of very fine to fine-grained sandstone with a maximum thickness of about 300 m (McGuire, 2017). Due to the fine-grained nature of the Arikaree and Brule formations, they may or may not be hydraulically connected to overlying geologic units. The Cretaceous Pierre Shale forms the impermeable base of the High Plains Aquifer in the NSH.

Although the NSH has the greatest volume of saturated sediment in the High Plains aquifer and least net groundwater declines (Haacker et al., 2016; McGuire, 2017; Peterson et al., 2016; Scanlon et al., 2012), the area is vulnerable to climate change, irrigation, and Redcedar (*Juniperus virginiana*) encroachment (Adane et al., 2019; Burbach and Joeckel, 2006; Loope and Swinehart, 2000; Suttie et al., 2005; Zou et al., 2018). For example, irrigation wells increased from only a few hundred in 1940 to 7775 within a 10 km buffer of NSH in 2019 (Nebraska Department of Natural Resources, 2019). Research suggests that the change in supply and demand of precipitation and evapotranspiration can decrease recharge by 25–50% and lead to desertification (Adane et al., 2019; Peterson et al., 2020). With 23 continuous observation wells, and 61 seasonal and annual wells, the spatial variability present in the groundwater level is difficult to characterize. As such, the annual Nebraska Statewide Groundwater Level Monitoring Report only provides partial groundwater level change information for the NSH region (Young et al., 2019). Similarly, the most widely used water table elevation maps of spring 1995 (hand-drawn) and 2012 (natural neighbor interpolation) from the NSH region are based on limited observations (Rossman et al., 2018) and uses method that do not account for the associated uncertainty. This study, therefore, provides an alternative approach to assess the spatial variability of groundwater level in the NSH using remote measurement of the water level in thousands of shallow endorheic lakes.

2.2. Dataset

The study uses Sentinel-2 satellite images to delineate the boundary between the lake and land surface area. Sentinel-2, a constellation of Sentinel-2a and Sentinel-2b satellites operated by the European Union Copernicus program, has a spatial resolution of 10, 20, and 60 m with 13 spectral bands in the visible, near infrared, and shortwave infrared region. The revisit frequency of each single satellite is 10 days, and the combined constellation revisit is 5 days. The level 2A images, used in the study, are bottom-of-atmosphere reflectance values corrected for radiometric, geometric, and atmospheric effects.

The LIDAR point cloud data was collected by United States Geological Survey (USGS) in 2016 and 2017 (hatched lines in Fig. 1) in the NSH. The LIDAR data has an aggregate nominal pulse spacing of ≤ 0.71 m and an aggregate nominal pulse density of ≥ 2 points per m^2. The level 2 (QL2) data used in the study has an absolute vertical accuracy of ≤ 10 cm root mean square elevation (RMSEz) with NAVD88 and NAD83 as a vertical and horizontal datum, respectively. We downloaded point cloud through the USGS FTP server and used FUSION tools (McGaughey, 2009) to clip, filter, and merge within the buffered boundary of lakes. The time of LIDAR data, Sentinel-2 satellite images, and observation wells were matched such that the water levels are measured at a similar timeframe. The areas with missing point cloud (Fig. 1) data were filled from 1 m resolution digital elevation model derived from LIDAR data.

The study also uses data from observation wells (Fig. 1). The observation well data were hosted in the database maintained by the Conservation and Survey Division, School of Natural Resources, University of Nebraska-Lincoln, and the Nebraska Department of Natural Resources. These data have been checked for quality and consistency (Young et al., 2019). The 23 observation wells have hourly measurements of the depth to water from the land surface. The depth to water from the land surface was then subtracted from the surveyed elevation of the land surface to obtain the elevation of the water table or potentiometric surface. **Fig. 2** shows the overall method used to derive the lake groundwater variation in the NSH.

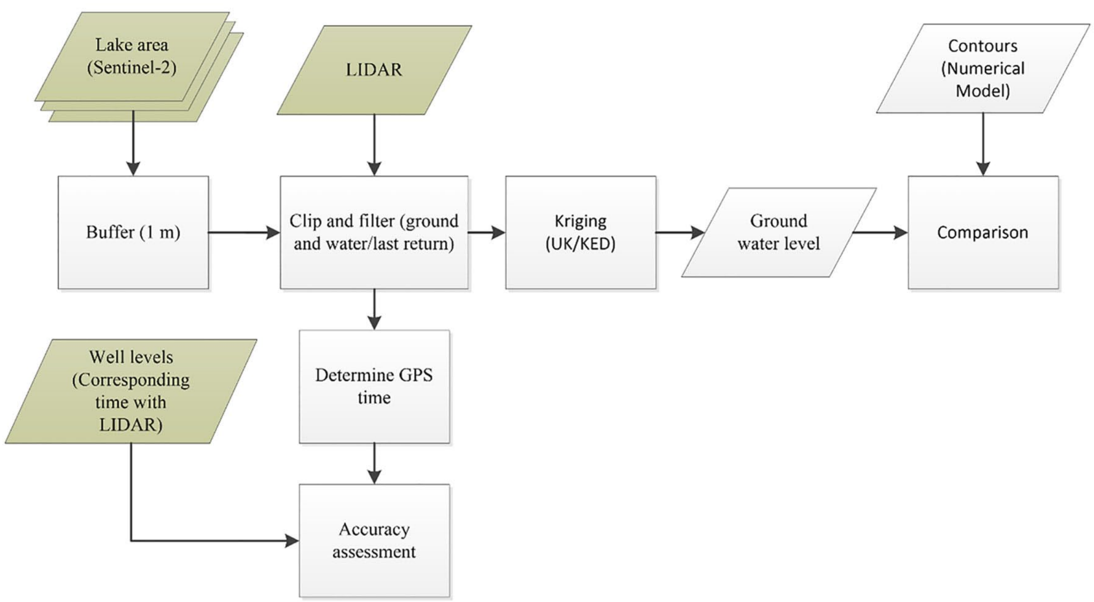

Fig. 2. Methodological framework for predicting the groundwater level derived from lake groundwater level using LIDAR data. Green color shows the data that were matched for time.

2.3. Lake area delineation

The visible and near infrared bands of Sentinel-2 images, hosted in Google Earth Engine (Gorelick et al., 2017), were filtered for cloud cover less than 10% and were mosaicked using median values for May to June 2017 in correspondence with LIDAR data acquisition time. The mosaicked images were transformed using tasseled cap coefficients derived from Sentinel images (Shi and Xu, 2019). The brightness, greenness, and wetness components were stacked with original bands and classified into water and non-water pixels using a random forest classifier in Google Earth Engine. The tasseled cap transformation reduces the influence of shadows and enhances water area detection and delineation (Zhuang and Chen, 2018) whereas the original bands provide the classifier with spectral variability present in water areas. Random forest classifier, an ensemble of decision trees, provides higher accuracy and is widely used in processing remotely sensed imagery, including water and wetland classification (Shrestha et al., 2021; Tian et al., 2016; Wang et al., 2018, 2020). The classifier was trained using samples collected through visual image interpretation of National Agriculture Imagery Program (NAIP) with 75% training (287) and 30% testing (109) set. The classified image was converted into a shapefile and exported for further analysis. Lakes with an area less than 0.008 km^2 were filtered and removed to reduce the effect of smaller misclassified pixels due to the ephemeral water areas that form near lakes and wetlands. The smaller lakes were also removed to avoid the effect of clustering and overfitting the variogram (Goovaerts, 1997). Similarly, lakes with a higher perimeter to area ratio were filtered to reduce the triangular and irregular-shaped polygons. The lakes were then buffered by 1 m to reduce the effect of missing LIDAR point cloud from water due to low backscatter.

2.4. Lake surface water level estimation and validation

Lake surface water level was estimated by combining the lake boundary and LIDAR point cloud using the waterline method. The waterline method, mainly used to evaluate the water level changes in coastal areas and lakes (Bell et al., 2016; Kang et al., 2017; Qi et al., 2019; Yue and Liu, 2019; Zhang et al., 2020), superimposes the boundary between the water surface and landmass on the elevations

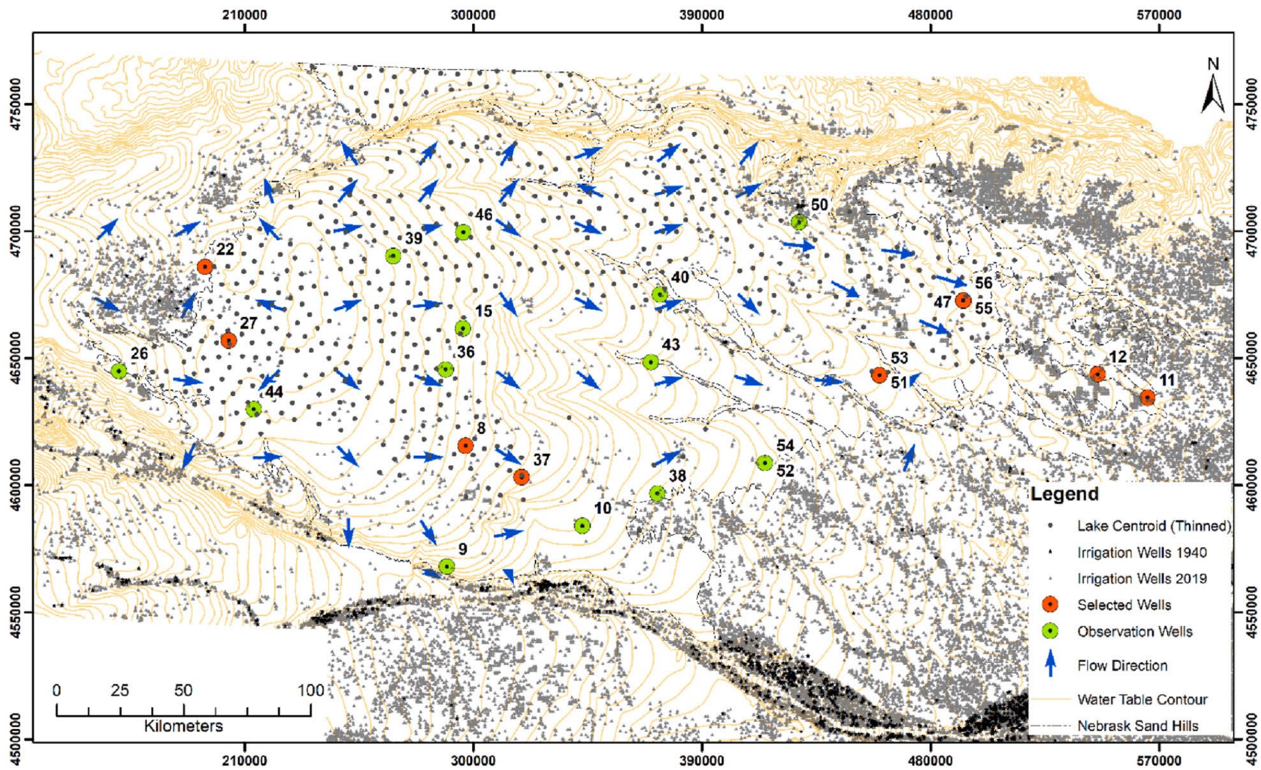

Fig. 3. Determining the lakes and observation wells for comparison using flow direction, separation distance and ambient gradient correction.

relative to mean sea level. The overall process involves the following: (i) delineate lake boundaries from Sentinel-2 images and create a 1 m buffer; ii) superimpose the buffered lake boundary with the LIDAR point cloud to clip and filter the last returned LIDAR points; and (iii) calculate the minimum, maximum and mean value that represents the lake water level or lake groundwater level. Given the gentle dune topography, the boundary between the lake and land surface is assumed to transition smoothly, therefore, a difference greater or equal to 5 m between the minimum and maximum LIDAR point cloud within the buffer was filtered as outliers. The outliers were considered errors associated with an inaccurate representation of the boundary derived from Sentinel-2 images. A total of 2300 lakes were retained and converted to points for geostatistical analysis. **Fig. 3** shows the lakes (thinned for visualization) clusters at the western and northern part of the NSH while fewer or no lakes are present in the southern part. The points that represent reservoirs or man-made impoundments were manually removed.

The lake groundwater level derived from LIDAR data were validated against the water level from the observation wells. The lakes and observation wells were selected (Fig. 3) based on the following criteria: i) water level measurements from the observation wells were matched up with the time the LIDAR point cloud was collected; ii) since the lake water level represents the unconfined aquifer, any wells that penetrated the confined aquifer, based on the well drilling profile, were filtered; and iii) lakes nearest and along the regional groundwater flow direction were retained. The selected lakes were corrected for ambient hydraulic gradient and then compared with water levels in the observation wells. In general, the LIDAR data were acquired between May and June of 2017 and therefore represents the spring season or pre-stress groundwater level. Of the 23 observation wells, only eight were used and compared to the nearest lake level elevation. The other 15 observation wells were not used for the following reasons: four wells penetrated the confined aquifer and thus the water didn't interact directly with the lakes; three wells were farther than 20 km from any lake; four wells were missing LIDAR data, and four wells data were missing at the time of LIDAR data collection.

2.5. *Geostatistical estimation and prediction*

Geostatistic-based methods were used to estimate and predict the lake groundwater level in the NSH. Geostatistics uses the sampled attribute Z at location s_i to estimate the Z at unsampled location s_o. The observation is decomposed into the mean and the stochastic component (random variable) as in Eq. (1). The mean or the trend component $\mu(s)$ is estimated either using the polynomial functions (UK) or auxiliary information such as elevation (KED) (Desbarats et al., 2002; Goovaerts, 1997). The spatial dependence between the observations is estimated from residuals (stochastic component) using semivariogram and predicted for the unsampled locations. Additional detail on UK and KED equations are provided in Desbarats et al. (2002); Deutsch and Journel (1992), and Goovaerts (1997).

$$Z(s) = \mu(s)+Z(s) \tag{1}$$

We used UK and KED to estimate and predict the lake groundwater level variation in the NSH. The lake groundwater level was checked

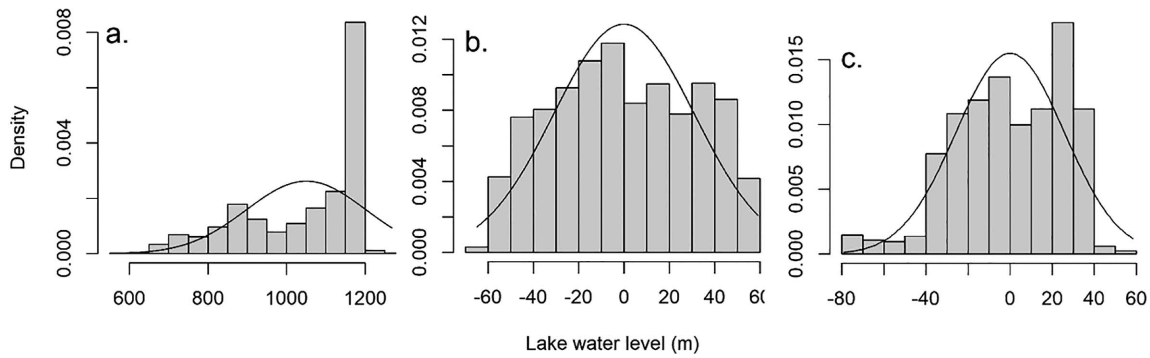

Fig. 4. Distribution of lake groundwater level for a) raw data, b) residuals of first order polynomial c) second order polynomial.

for normality using histogram plots, skewness, and kurtosis coefficients. The test showed that the raw data are skewed towards the left (**Fig. 4**a) with a skewness coefficient of −0.89 and a kurtosis of 2.55. A skewness value closer to zero and kurtosis closer to 3 indicates a normal distribution.

2.6. Universal kriging

UK is used when the data shows the presence of regionalized variables. A semivariogram analysis of raw data (not shown here) shows the presence of a regional trend, therefore, first and second order polynomials were used to estimate the trend from the lake groundwater level. A first and second order polynomial fit explained 96 and 98% of the variance present in the lake groundwater level, respectively. Similarly, the histogram plot (Fig. 4b, c) and skewness coefficient of 0.02 and −0.51 and kurtosis coefficient of 1.93 and 2.77 for the residuals of first and second-order polynomials, respectively, indicate a distribution closer to normal. Therefore, we used a second order polynomial fit to remove the trend and estimate the residuals for further analysis.

The initial values of nugget, range, and sill were determined from the visual analysis of a semivariogram plot. Theoretical semivariogram models such as spherical, Gaussian, exponential, and Bessel (Cressie and Wikle, 2015; Deutsch and Journel, 1992; Gringarten and Deutsch, 2001) were fitted to the empirical lake groundwater level data

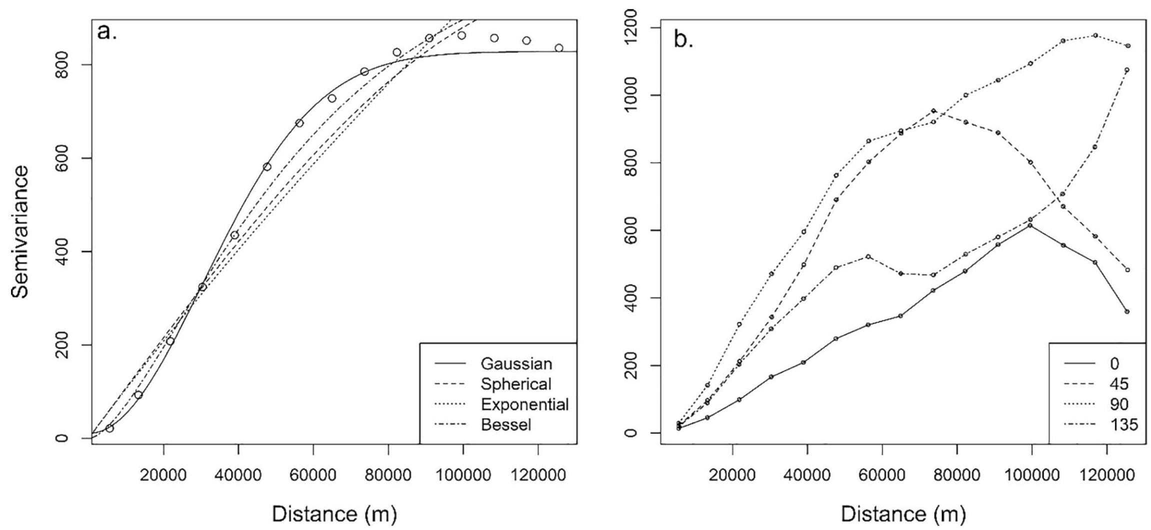

Fig. 5. Semivariance and directional semivariance for universal kriging.

(**Fig. 5**a). The model with the lowest residual sum of squares (RSS) were used for modelling the spatial correlation structure. Anisotropy present were checked using directional variograms at four main directions (0, 45, 90, and 135) with an angle of tolerance of ± 22.5 (Goovaerts, 1997). Fig. 5b shows the presence of anisotropy that were corrected using the angle and scaling factor. The prediction was performed in 90 m resolution grid.

2.7. Kriging with an external drift

The drift present in the lake groundwater level was estimated using the bare earth digital elevation model of 90 m resolution. Regression analysis between lake groundwater level and topography was used to determine the association of dependent and independent variables. The results show that the lake water level was highly linear with the elevation ($R^2 > 0.95$). As with the UK, the theoretical models with the least RSS were used to determine the spatial correlation structure (**Fig. 6**a). The semivariogram of residuals after trend removal does not show the presence of trend and anisotropy (Fig. 6b). The optimal resolution for KED prediction was determined by predicting and evaluating the surface at 90, 200, 500, 700, and 1000 m grids. The

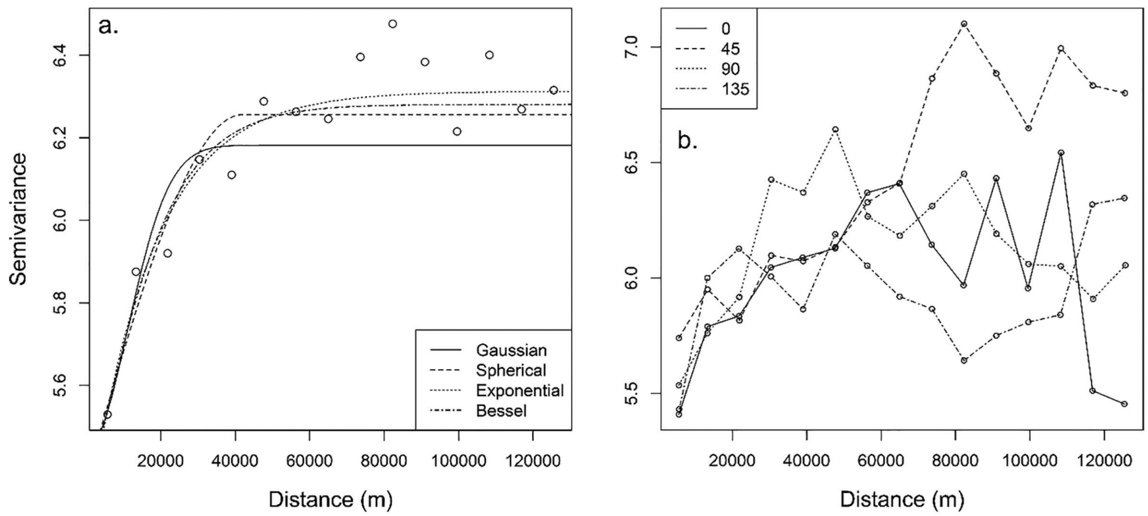

Fig. 6. Semivariogram and directional semivariogram using kriging with an external drift.

higher resolution grids (<90 m) were overwhelmed with the local topographic variation and resulted in noisy lake groundwater level. A coarser-resolution topography (>500 m) averaged the local groundwater level variation. Therefore, a 200 m grid was selected as optimal resolution for KED.

We used the gstat package (Pebesma and Graeler, 2013) to implement the UK and KED approach to map the groundwater level variation in the NSH.

2.8. Validation

The K-fold cross-validation measure was used to determine the accuracy of the predicted surface. The method divides the data into multiple sets, one subset is used to test while the other is used to predict. Based on the results of the cross-validation, the following evaluation statistics were used to compare the accuracy of the interpolation. Mean square error (MSE) is sensitive to outliers as it measures the magnitude of the error. Root mean square error (RMSE) provides a standard deviation of the residuals. The mean squared deviation ratio (MSDR) is the mean of the ratio of the squared prediction errors to the variance. A MSDR close to one indicates a good model. Modified index of agreement (MD) is the ratio between the mean square error and the potential error. MD is like root mean square error with a value between 0 and 1. Residual prediction deviation (RPD) is the standard deviation of the observation divided by the root mean square error of prediction. A higher RPD value shows good prediction. Residual sum of squares (RSS) is used to evaluate the degree of fitting between the empirical and theoretical variogram models.

$$MSE = \frac{1}{n} \sum_{i=1}^{n} \left[\hat{z}(s_i) - z(s_i)\right]^2 \tag{2}$$

$$RSS = \sum_{i=1}^{n} \left[\hat{z}(s_i) - z(s_i)\right]^2 \tag{3}$$

$$RMSE = \sqrt{\frac{1}{n} \sum_{i=1}^{n} \left[\hat{z}(s_i) - z(s_i)\right]^2} \tag{4}$$

$$MSDR = \frac{1}{n} \sum_{i=1}^{n} \frac{\left[\hat{z}(s_i) - z(s_i)\right]^2}{\hat{\sigma}^2(s_i)} \tag{5}$$

$$MD = 1 - \frac{\sum_{i=1}^{n} \left|z(s_i) - \hat{z}(s_i)\right|^2}{\sum_{i=1}^{n} \left(\left|\hat{z}(s_i) - \overline{z(s_i)}\right| \left|z(s_i) - \overline{z(s_i)}\right|\right)} \tag{6}$$

$$RPD = \frac{\sqrt{\frac{1}{n} \sum_{i=1}^{n} \left[z(s_i) - \overline{z(s_i)}\right]^2}}{\sqrt{\sum_{i=1}^{n} \left|z(s_i) - \hat{z}(s_i)\right|}} \tag{7}$$

The lake groundwater level derived from UK was validated against the contour from a comprehensive regional groundwater flow model. Rossman et al. (2018) developed a two-dimensional numerical groundwater flow model to simulate the hydraulic head distribution in the groundwater-fed lakes system for the entire NHS. They represented the High Plains aquifer as a single layer with spatially varying hydraulic conductivities with a satellite-derived distributed recharge applied from the top surface. A finite-difference numerical groundwater modeling code, MODFLOW, was used to solve the governing groundwater flow equations under steady-state conditions using a 1 km uniform horizontal grid discretization. Recharge and hydraulic conductivities were calibrated using a non-linear automated calibration code, PEST

(Parameter ESTimation). A strong correlation coefficient of 0.99 was attained between simulated and observed heads after the PEST calibration. Even though the hydrostratigraphy was represented as a single layer, the numerical modeling approach captured the groundwater heads in the High Plains aquifer in the NHS. Details on the model can be found in Rossman et al. (2018).

The result of KED was compared against the groundwater level contour of spring 2012 derived by the Conservation and Survey Division of the School of Natural Resources, University of Nebraska-Lincoln. The contours were generated using the natural neighbor interpolation method (Gilmore et al., 2019) that preserves the local variation of the groundwater level and were comparable with the results of KED.

The accuracy of extracted lake area was validated using the overall accuracy and Kappa statistics (Stehman, 1997). The samples were generated randomly and labeled using visual image interpretation of NAIP.

3. Results

3.1. Accuracy of lake area and lake groundwater level

Lake area accuracy assessment shows an overall accuracy of 95%. A Kappa statistic of 0.94 shows that the lake's boundary is delineated better than chance. The water level in the observation wells, at the time of LIDAR data acquisition, were compared with the minimum, maximum, and mean lake groundwater level. The results (**Table 2**) show that the lowest mean square error (MSE) was the maximum lake groundwater level and is twice as accurate as the mean and the minimum value. The lakes on the southern (Well ID 37) and easternmost part (Well ID 11, 12, and 51) (Fig. 1) of the NSH had the largest error. It is hypothesized that this is due to the pumping from irrigation wells and groundwater flow direction (Shrestha et al., 2021) (Fig. 3). The low MSE highlights that the lake water level provides sufficient accuracy to characterize the groundwater levels in the NSH and the LIDAR data can be used to characterize the short-term as well as long-term water level variation.

Table 2 Comparison of LIDAR estimated groundwater levels and water levels in observation wells at the corresponding time (m.a.s.l. = meters above sea level).

Well ID	*Water Level (m.a.s.l.)*	*LIDAR water level (m)*			*Gradient*	*Distance*	*Correction factor*	*Corrected water level (m)*			*Difference (m)*		
		min.	*max.*	*mean*	*i*	*L*	*i*L*	*min.*	*max.*	*mean*	*min.*	*max.*	*mean*
8	1069.66	1067.35	1068.04	1067.44	0.0011	1490	1.60	1068.95	1069.64	1069.04	0.71	0.01	0.62
27	1184.97	1183.22	1184.22	1183.32	0.0006	958	0.58	1183.80	1184.80	1183.90	1.18	0.17	1.08
37	1012.52	1012.55	1013.67	1012.80	0.0035	560	1.96	1010.59	1011.71	1010.84	1.94	0.81	1.68
22	1186.02	1184.17	1184.34	1184.25	0.0003	3462	1.19	1185.36	1185.53	1185.43	0.66	0.49	0.59
51	737.15	737.16	737.34	737.22	0.0019	337	0.65	737.81	737.99	737.87	−0.66	−0.84	−0.72
47	711.15	703.05	703.83	703.41	0.0024	2797	6.81	709.86	710.63	710.21	1.30	0.52	0.94
11	578.16	578.67	578.76	578.74	0.0021	160	0.34	579.01	579.10	579.08	−0.85	−0.94	−0.92
12	618.43	611.96	612.05	612.01	0.0027	2118	5.72	617.67	617.77	617.72	0.76	0.66	0.71
MSE	1.18	0.4	0.93										

3.2. Spatial dependence of lake groundwater level

The semivariogram analysis reveals that the Gaussian model provides the best fit for UK (**Table 3**) with RSS of 0.27 while the Bessel, spherical and exponential models have RSS of 0.95, 5.03, and 6.19, respectively. Similarly, the exponential model has the lowest RSS of 0.00000609 followed by Bessel, spherical and Gaussian for KED (Table 3). Sill variance is consistent with all the theoretical semivariogram models for KED while it varies for UK. KED shows a smaller range such that the semivariogram flattens at shorter distances than the UK. A nugget-to-sill ratio of 0.013 for UK shows higher spatial dependence while 0.83 for KED showed a weak spatial dependence. A variable has strong dependence when the nugget-to-sill ratio is less than 0.25, moderate dependence with values between 0.25 and 0.75, and weak dependence with values >0.75 (Liu et al., 2006).

Table 3 Comparison of theoretical variogram model parameters between universal kriging and kriging with an external drift using residual sum of squares.

Theoretical models	Variogram parameters							
	Nugget		Sill		Range		RSS	
	UK	KED	UK	KED	UK	KED	UK	KED
Gaussian	10.35	5.45	818.13	6.18	43,143	15,656	0.27	1.35e−5
Bessel	0	5.38	1081.51	7.16	38,554	11,307	0.95	7.49e−6
Spherical	0	5.37	960.96	6.25	132,775	41,809	5.03	1.08e−5
Exponential	0	5.24	3390.28	6.31	315,374	17,403	6.19	6.09e−6

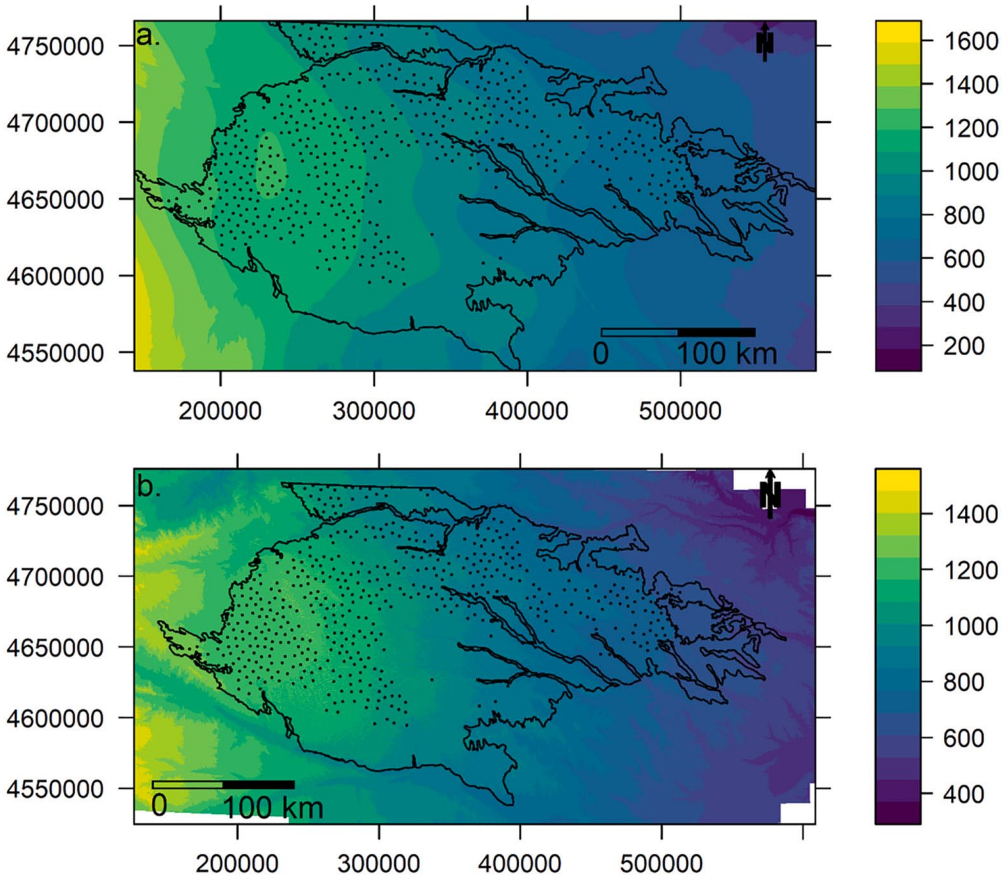

Fig. 7. Predicted lake water level using a) universal kriging b) kriging with an external drift.

3.3. Groundwater level prediction

The predicted map illustrates the spatial variability present in the groundwater level. The western part contains higher groundwater elevation while the eastern part of NSH contains the lowest elevation (**Fig. 7**). The UK approach that uses second order polynomial as trend surface provides smoother water level variation (Fig. 7a) that resembles the regional water flow regime. Predicted KED surface (Fig. 7b), however, reveals the local variation in the groundwater level. The streams, along with areas with little or no observations, are better represented by KED as compared to UK. The advantage of UK is that no external variables are necessary to remove the trend and it is easy to implement. KED, however, requires external variables to be linearly correlated with the groundwater level and must be present at the sampled and unsampled locations.

Table 4 Performance measures comparison between the universal kriging and kriging with an external drift.

Method	*Performance measures*				
	MSE (m^2)	*RMSE (m)*	*MSDR*	*RPD*	*MD*
UK	0.007	4.46	1.49	0.71	1
KED	−0.003	2.39	1.01	1.32	1

A 10-fold cross-validation result shows that both UK and KED are unbiased with a mean error estimate closer to zero. UK shows a slightly higher RMSE of 4.46 m compared to 2.39 m of KED. KED confirms better prediction with better MSDR, RPD, and MD than UK (**Table 4**). The Taylor diagram (**Fig. 8**) also highlights that KED provides a better approximation of groundwater level than the UK. The standard deviation map (**Fig. 9**) shows the error distribution of the kriging interpolation at NSH. The southern and eastern part of NSH shows higher error both in UK (Fig. 9a) and in KED (Fig. 9b) where there are fewer lakes. KED, however, shows lower standard deviation as the digital elevation model effectively removed the regional trend present in the data as compared to second-order polynomials fitting of UK.

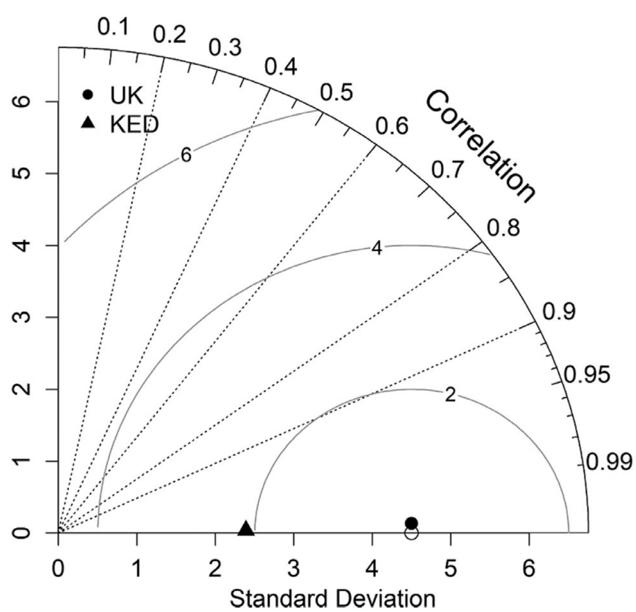

Fig. 8. Taylor diagram showing the universal kriging and kriging with an external drift.

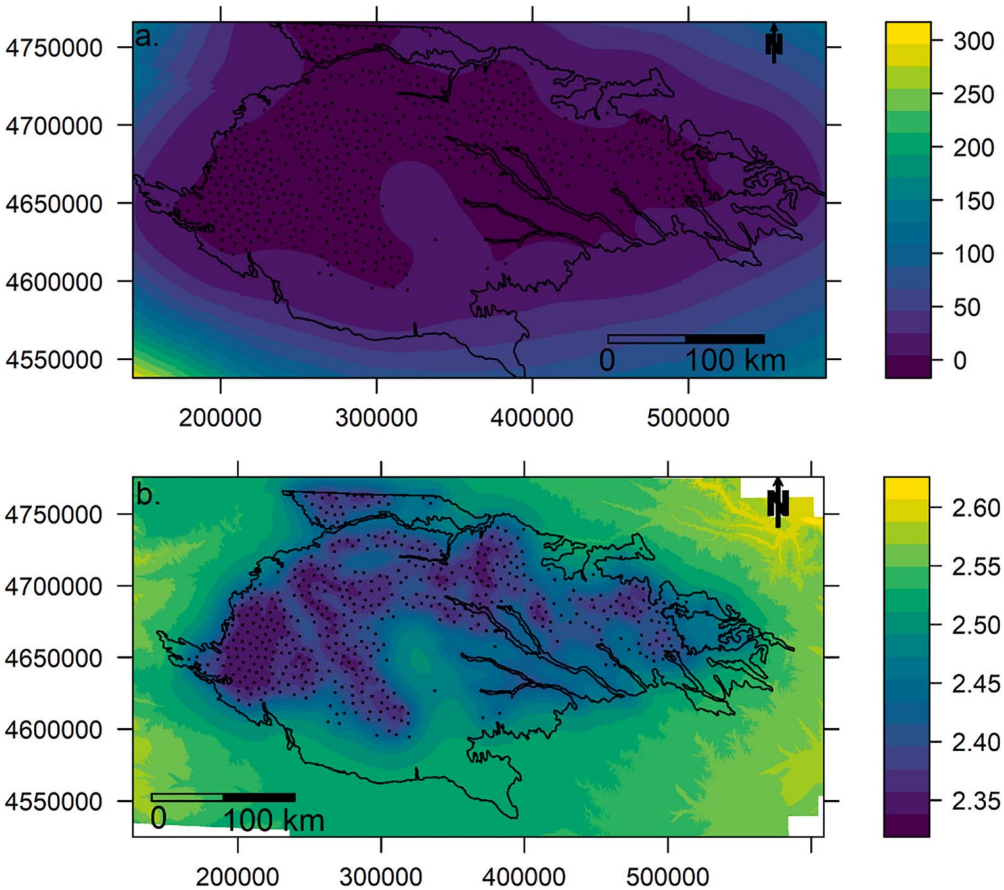

Fig. 9. Standard deviation error distributing for a) universal kriging b) kriging with an external drift.

Comparison between the contour lines generated using UK and the numerical model shows a high degree of correspondence. **Fig. 10**a shows that the hydraulic head contours match with lake groundwater level contours especially in the western part of the NSH where the lake density is higher. In the parts where the head distributions are dominated by river-aquifer interactions, contours were less likely to match as the river aquifer interaction in the numerical model was represented by a head-dependent flux boundary, which resulted in a better estimation of the head near the stream network. The difference could be attributed to the limitation of kriging that the groundwater flow is not necessarily conserved and fails to reproduce features such as boundary conditions (Rivest et al., 2008; Tonkin and Larson, 2002).

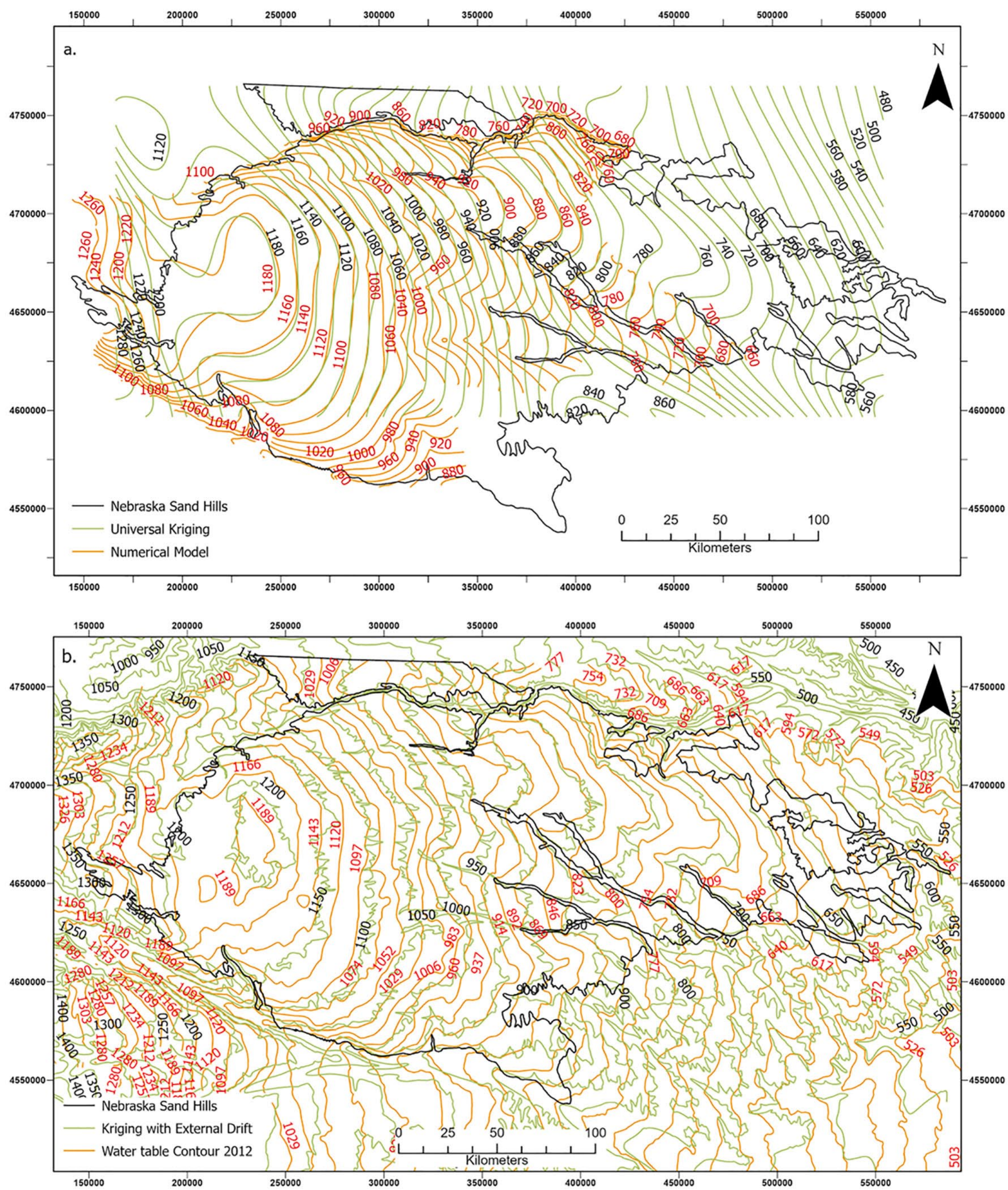

Fig. 10. Contour comparison a) universal kriging and regional numerical groundwater flow model b) kriging with an external drift and natural neighbor contour 2012.

KED-generated contours and 2012 water table contours do not agree in many areas (Fig. 10b). The KED, with a large number of lake groundwater level observations (>2300), provides a better characterization of groundwater level and captures the trend and general pattern seen in the water table contours from 2012. KED also captured the variation along streams not well captured in UK. The dissimilarity in water table contours may be due to the difference in methods and the number of hydraulic head measurements used for interpolation. The contours of 2012 were generated using the natural neighbor interpolation technique for the spring season (Gilmore et al., 2019) with fewer observation wells and some information from smaller scale contour maps (A. Young, personal communication, 2020).

4. Discussion

The results of this study show that the lake groundwater level derived using topographic LIDAR provides an accurate representation of groundwater levels in the NSH. With lake water levels lower than the regional potentiometric surface and evaporation significantly higher than precipitation, the lakes, in general, are areas of focused groundwater discharge (Gosselin et al., 2000; Winter, 1986; Zlotnik et al., 2009). Although the lake groundwater level follows the surface terrain at the regional scale, significant differences are observed near lakes at local scales (Winter, 1999) as seen on the predicted surface from UK and KED. Locally, lake position, in relation to the regional groundwater flow regime and the gradient between the regional and local head, determines whether a lake gains or loses water from the groundwater system (Born et al., 1979; Zlotnik et al., 2009). For example, when lakes are closely spaced and are on a hummocky topography, transient groundwater mounds forms. The presence of groundwater mounds induces groundwater flow towards the lake while the absence of mounds induces the water to flow away from the lake leading to a change in lake water levels (Gosselin and Khisty, 2001; Winter, 1999). Seasonal changes in groundwater configuration also alters the location, magnitude, and direction of groundwater flow into or out of the lake (Winter, 1986). At a regional scale, however, the water table elevations in the NSH show minor spatiotemporal trends (<±2m) since predevelopment (1953) and between 2001 and 2015 (Korus et al., 2010; McGuire, 2017). The accuracy of lake groundwater level derived from topographic LIDAR was based on eight observation wells. A larger number of observation wells distributed across the study area would provide a better estimate of the groundwater level. In this study, however, only eight observation wells satisfied the conditions defined in section 2.4. Besides the number and distribution of the observation wells, the estimated lake water level depends on the: i) accuracy of the boundary between the lake and adjacent landmass derived from satellite images, ii) strength of backscatter from topographic LIDAR from water areas, and iii) response of water level due to hydraulic stresses caused by drought or irrigation demand from neighboring irrigation wells. The accuracy assessment shows that the Sentinel-2 images with spatial resolution of 10 m provides proper representation of the lake area for the study. However, higher resolution satellite or aerial images such as National Agriculture Imagery Program would reduce the uncertainty associated along the boundary between lake and landmass. Similarly, the waterline method reduces uncertainty associated with the low backscatter and laser dropout of topographic LIDAR at deeper water. The response of a local groundwater system to stress is dependent on the depth to water, thickness and geologic composition of the unsaturated zone and the hydraulic characteristics of the aquifer (Burbach and Joeckel, 2006). For example, the lake responses suggest the unconfined aquifer in the NSH has shorter response times (5–10 years) (Rossman et al., 2014; Shrestha et al., 2021) compared to confined aquifer (hundreds of years).

The semivariogram analysis of raw lake groundwater level reveals the presence of a regional trend. The regional trend present in the groundwater level overwhelms the local variation (Kitanidis, 1997) and therefore has to be removed before using kriging (Goovaerts, 1997). Although the second order polynomial fitting in UK removes the trend, it still shows the presence of anisotropy in the direction of groundwater flow. The use of topography in KED effectively removes the trend and anisotropy (Fig. 6b) and captures the local variation present in the groundwater level. Therefore, the use of topography as an explanatory variable provides a simple and powerful method to capture the local variation present in an area. However, in areas with sparse observation data, secondary topographic features can cause undesirable variation in the interpolated water level when the drift captures the random and short-scale fluctuations rather than the larger-scale variations (Desbarats et al., 2002; Rivest et al., 2008). The presence of sand dunes in the digital elevation model created an unrealistic representation of groundwater levels. Therefore, several representations of topography (Desbarats et al., 2002) at 90, 200, 500, 700, and 1000 m, were used to determine the appropriate relationship between the water table elevation and topography. Wolock and Price (1994) found that the coarser topographic representations more accurately represent the water table configuration that are smoother than the land surface topography. UK captured the regional pattern of groundwater level variation (Fig. 7a) similar to the results of the regional scale steady-state groundwater flow model. The comparison between the contours generated using UK and the numerical model shows good correspondence in areas with a large number of lake groundwater level observations. Although the KED and 2012 contour maps do not match perfectly, they depict the magnitude and patterns of the groundwater level variation. The difference in contours may be due to the use of different interpolation method, number of hydraulic head measurement, and change in water level between 2012 and 2017. For example, the groundwater level increased by 0.6 – 3 m from spring 2013 to spring 2018 in the NSH (Young et al., 2019).

Since the method has been validated with observation wells, future work can use Sentinel-2 images to create monthly or bi-monthly water table maps. This can be used to update managers with the status of the water depth and calibrate a transient groundwater model across the NSH. To apply this method, the lake level would have to be equal to or greater than the water level measured by LIDAR. Alternatively, bathymetry survey could be integrated with LIDAR to create lakebed map and use it for estimating the lake groundwater level at regular intervals. The method is applicable in semi-arid and arid regions of North America, Africa (Carter, 1995), Asia (Chen et al., 2004; Ma and Edmunds, 2006), Europe (Heine et al., 2015; Sacks et al., 1992), and Australia (Turner and Townley, 2006; Tweed et al., 2009) that hosts closed lakes with dominant groundwater hydrology. The method may work with lakes in glaciated terrain composed of unconsolidated and permeable materials and connection to local and intermediate groundwater flow system (e.g., (Holzbecher, 2001; Hunt et al., 2013; Lischeid et al., 2010; Merz and Pekdeger, 2011; Speldrich et al., 2021)). The method can be tested in several geomorphological settings with lake (closed) hydrology primarily dominated by groundwater influx.

5. Conclusion

The study shows that the LIDAR data accurately represents the groundwater level in the Nebraska Sand Hills (NSH). The integration of optical and LIDAR sensor compensates each other and significantly increases the hydraulic head observations to characterize the spatial correlation structure present in the groundwater of NSH. The study finds that kriging with an external drift (KED) provides better estimates of the groundwater level than universal kriging (UK) at unsampled locations. The use of topography as an explanatory variable captures the local variation present in the groundwater level. A higher correspondence of the predicted surface with a numerical model derived hydraulic head highlights the LIDAR derived lake groundwater level can calibrate or define the boundary conditions in numerical models. The method can be applied to other areas where the surface water represents the groundwater level.

With the possibility of LIDAR instruments to mount on a platform near lakes or use current LIDAR data, the study also provides a framework to monitor the groundwater level in the NSH at high spatial and temporal resolution. Similarly, the study also provides the prospect to combine the high spatial resolution digital elevation model and bathymetry survey and thereby use lakes as observation wells for future research.

CRediT authorship contribution statement

Nawaraj Shrestha: Data curation, Methodology, Formal analysis, Writing - original draft, Visualization.

Aaron R. Mittelstet: Conceptualization, Writing - review & editing, Supervision, Funding acquisition.

Aaron R. Young: Writing - review & editing.

Troy E. Gilmore: Conceptualization, Writing - review & editing.

David C. Gosselin: Writing - review & editing.

Yi Qi: Writing - review & editing.

Caner Zeyrek: Writing - review & editing.

Competing Interest The authors declare that they have no known competing financial interests or personal relationships that could have appeared to influence the work reported in this paper.

Acknowledgments The authors acknowledge the U.S. Department of Agriculture - National Institute of Food and Agriculture (Hatch project 1015698), Robert B. Daugherty Water for Food Global Institute at the University of Nebraska-Lincoln and the Water Sustainability Fund, Nebraska Natural Resource Commission. We would like to thank the editors and anonymous reviewers for constructive suggestion and feedback.

References

Adane, Z., Zlotnik, V.A., Rossman, N.R., Wang, T., Nasta, P., 2019. Sensitivity of potential groundwater recharge to projected climate change scenarios: A site-specific study in the Nebraska Sand Hills, USA. Water (Switzerland) 11, 950. https://doi.org/10.3390/w11050950

Adhikary, P.P., Dash, C.J., 2017. Comparison of deterministic and stochastic methods to predict spatial variation of groundwater depth. Appl. Water Sci. 7 (1), 339–348. https://doi.org/10.1007/s13201-014-0249-8

Ahlbrandt, T.S., Fryberger, S.G., 1980. Eolian deposits in the Nebraska sand hills. US Geol. Surv. Prof. Pap. 1120, 1–24.

Ahmadi, S.H., Sedghamiz, A., 2008. Application and evaluation of kriging and co-kriging methods on groundwater depth mapping. Environ. Monit. Assess. 138 (1-3), 357–368. https://doi.org/10.1007/s10661-007-9803-2

Ahmadi, S.H., Sedghamiz, A., 2007. Geostatistical Analysis of Spatial and Temporal Variations of Groundwater Level. Environ. Monit. Assess. 129 (1-3), 277–294. https://doi.org/10.1007/s10661-006-9361-z

Ahmed, S., 2007. In: Groundwater. Springer Netherlands, Dordrecht, pp. 78–111. https://doi.org/10.1007/978-1-4020-5729-8_4

Asadzadeh Jarihani, A., Callow, J.N., Johansen, K., Gouweleeuw, B., 2013. Evaluation of multiple satellite altimetry data for studying inland water bodies and river floods. J. Hydrol. 505, 78–90. https://doi.org/10.1016/j.jhydrol.2013.09.010

Balázs, B., Bíró, T., Dyke, G., Singh, S.K., Szabó, S., 2018. Extracting water-related features using reflectance data and principal component analysis of Landsat images. Hydrol. Sci. J. 63 (2), 269–284. https://doi.org/10.1080/02626667.2018.1425802

Bell, P.S., Bird, C.O., Plater, A.J., 2016. A temporal waterline approach to mapping intertidal areas using X-band marine radar. Coast. Eng. 107, 84–101. https://doi.org/10.1016/j.coastaleng.2015.09.009

Bijeesh, T.V., Narasimhamurthy, K.N., 2020. Surface water detection and delineation using remote sensing images: a review of methods and algorithms. Sustain. Water Resour. Manag. 6, 68. https://doi.org/10.1007/s40899-020-00425-4

Boezio, M.N.M., Costa, J.F.C.L., Koppe, J.C., 2006. Kriging with an external drift versus collocated cokriging for water table mapping. Trans. Institutions Min. Metall. Sect. B Appl. Earth Sci. 115 (3), 103–112. https://doi.org/10.1179/174327506X138896

Born, S.M., Smith, S.A., Stephenson, D.A., 1979. Hydrogeology of glacial-terrain lakes, with management and planning applications. J. Hydrol. 43 (1-4), 7–43. https://doi.org/10.1016/0022-1694(79)90163-X

Buchanan, S., Triantafilis, J., 2009. Mapping water table depth using geophysical and environmental variables. Ground Water 47, 80–96. https://doi.org/10.1111/j.1745-6584.2008.00490.x

Burbach, M.E., Joeckel, R.M., 2006. A delicate balance: Rainfall and groundwater in Nebraska during the 2000–2005 drought. Gt. Plains Res. 16, 5–16.

Carter, R.C., 1995. Groundwater recharge and outflow patterns in a dunefield of North East Nigeria. Geomorphology and Groundwater. Wiley Chichester 157–176.

Chen, J.S., Li, L., Wang, J.Y., Barry, D.A., Sheng, X.F., Gu, W.Z., Zhao, X., Chen, L., 2004. Groundwater maintains dune landscape. Nature 432 (7016), 459–460. https://doi.org/10.1038/432459a

Condon, L.E., Maxwell, R.M., 2015. Evaluating the relationship between topography and groundwater using outputs from a continental-scale integrated hydrology model. Water Resour. Res. 51 (8), 6602–6621. https://doi.org/10.1002/2014WR016774

Cressie, N., Wikle, C.K., 2015. Statistics for spatio-temporal data. John Wiley & Sons.

Desbarats, A.J., Logan, C.E., Hinton, M.J., Sharpe, D.R., 2002. On the kriging of water table elevations using collateral information from a digital elevation model. J. Hydrol. 255 (1-4), 25–38. https://doi.org/10.1016/S0022-1694(01)00504-2

Deutsch, C. V, Journel, A.G., 1992. Geostatistical software library and user's guide. New York 119.

Döll, P., Hoffmann-Dobrev, H., Portmann, F.T., Siebert, S., Eicker, A., Rodell, M., Strassberg, G., Scanlon, B.R., 2012. Impact of water withdrawals from groundwater and surface water on continental water storage variations. J. Geodyn. 59–60, 143–156. https://doi.org/10.1016/j.jog.2011.05.001

Du, Z., Linghu, B., Ling, F., Li, W., Tian, W., Wang, H., Gui, Y., Sun, B., Zhang, X., 2012. Estimating surface water area changes using time-series Landsat data in the Qingjiang River Basin. China. J. Appl. Remote Sens. 6 (1), 063609. https://doi.org/10.1117/1.JRS.6.063609

Fernandez-Diaz, J.C., Glennie, C.L., Carter, W.E., Shrestha, R.L., Sartori, M.P., Singhania, A., Legleiter, C.J., Overstreet, B.T., 2014. Early results of simultaneous terrain and shallow water bathymetry mapping using a single-wavelength airborne LiDAR sensor. IEEE J. Sel. Top. Appl. Earth Obs. Remote Sens. 7 (2), 623–635. https://doi.org/10.1109/JSTARS.460944310.1109/JSTARS.2013.2265255

Gilmore, T.E., Zlotnik, V., Johnson, M., 2019. Recognition of regional water table patterns for estimating recharge rates in shallow aquifers. Groundwater 57 (3), 443–454. https://doi.org/10.1111/gwat.2019.57.issue-310.1111/gwat.12808

Goovaerts, P., 2000. Geostatistical approaches for incorporating elevation into the spatial interpolation of rainfall. J. Hydrol. 228 (1-2), 113–129. https://doi.org/10.1016/S0022-1694(00)00144-X

Goovaerts, P., 1997. Geostatistics for natural resources evaluation. Oxford University Press on Demand.

Gorelick, N., Hancher, M., Dixon, M., Ilyushchenko, S., Thau, D., Moore, R., 2017. Google Earth Engine: Planetary-scale geospatial analysis for everyone. Remote Sens. Environ. 202, 18–27. https://doi.org/10.1016/j.rse.2017.06.031

Gosselin, D.C., Khisty, M.J., 2001. Simulating the influence of two shallow, flow-through lakes on a groundwater system: implications for groundwater mounds and hinge lines. Hydrogeol. J. 9 (5), 476–486.

Gosselin, D.C., Rundquist, D.C., McFeeters, S.K., 2000. Remote monitoring of selected ground-water dominated lakes in the Nebraska Sand Hills. J. Am. Water Resour. Assoc. 36 (5), 1039–1051. https://doi.org/10.1111/jawr.2000.36.issue-510.1111/j.1752-1688.2000.tb05708.x

Gringarten, E., Deutsch, C.V., 2001. Teacher's aide: Variogram interpretation and modeling. Math. Geol. 33, 507–534. https://doi.org/10.1023/A:1011093014141

Gutentag, E.D., Heimes, F.J., Krothe, N.C., Luckey, R.R., Weeks, J.B., 1984. Geohydrology of the High Plains aquifer in parts of Colorado, Kansas, Nebraska, New Mexico, Oklahoma, South Dakota, Texas, and Wyoming (USGS, USA, groundwater). US Geol. Surv. Prof. Pap. https://doi.org/10.3133/pp1400B

Haacker, E.M.K., Kendall, A.D., Hyndman, D.W., 2016. Water Level Declines in the High Plains Aquifer: Predevelopment to Resource Senescence. Groundwater 54 (2), 231–242. https://doi.org/10.1111/gwat.2016.54.issue-210.1111/gwat.12350

Haitjema, H.M., Mitchell-Bruker, S., 2005. Are water tables a subdued replica of the topography? Ground Water 43, 781–786. https://doi.org/10.1111/j.1745-6584.2005.00090.x

Heine, I., Stüve, P., Kleinschmit, B., Itzerott, S., 2015. Reconstruction of lake level changes of groundwater-fed lakes in Northeastern Germany using rapid-eye time series. Water (Switzerland) 7, 4175–4199. https://doi.org/10.3390/w7084175

Höfle, B., Vetter, M., Pfeifer, N., Mandlburger, G., Stötter, J., 2009. Water surface mapping from airborne laser scanning using signal intensity and elevation data. Earth Surf. Process. Landforms 34 (12), 1635–1649. https://doi.org/10.1002/esp.v34:1210.1002/esp.1853

Hofton, M.A., Blair, J.B., Minster, J.-B., Ridgway, J.R., Williams, N.P., Bufton, J.L., Rabine, D.L., 2000. An airborne scanning laser altimetry survey of Long Valley, California. Int. J. Remote Sens. 21 (12), 2413–2437. https://doi.org/10.1080/014311600500030547

Holzbecher, E., 2001. The dynamics of subsurface water divides - Watersheds of Lake Stechlin and neighbouring lakes. Hydrol. Process. 15 (12), 2297–2304. https://doi.org/10.1002/(ISSN)1099-108510.1002/hyp.v15:1210.1002/hyp.261

Hopkinson, C., Crasto, N., Marsh, P., Forbes, D., Lesack, L., 2011. Investigating the spatial distribution of water levels in the Mackenzie Delta using airborne LiDAR. Hydrol. Process. 25, n/a-n/a. https://doi.org/10.1002/hyp.8167

Hunt, R.J., Walker, J.F., Selbig, W.R., Westenbroek, S.M., Regan, R.S., 2013. Simulation of Climate-Change Effects on Streamflow, Lake Water Budgets, and Stream Temperature Using GSFLOW and SNTEMP, Trout Lake Watershed, Wisconsin [WWW Document]. USGS Sci. Investig. Rep. 2013–5159 (accessed 6.9.21). https://pubs.usgs.gov/sir/2013/5159/

Jiang, Z., Qi, J., Su, S., Zhang, Z., Wu, J., 2012. Water body delineation using index composition and HIS transformation. Int. J. Remote Sens. 33 (11), 3402–3421. https://doi.org/10.1080/01431161.2011.614967

Kambhammettu, B.V.N.P., Allena, P., King, J.P., 2011. Application and evaluation of universal kriging for optimal contouring of groundwater levels. J. Earth Syst. Sci. 120 (3), 413–422. https://doi.org/10.1007/s12040-011-0075-4

Kang, Y., Ding, X., Xu, F., Zhang, C., Ge, X., 2017. Topographic mapping on large-scale tidal flats with an iterative approach on the waterline method. Estuar. Coast. Shelf Sci. 190, 11–22. https://doi.org/10.1016/j.ecss.2017.03.024

Kitanidis, P.K., 1997. Introduction to geostatistics: applications in hydrogeology. Cambridge University Press.

Korus, J.T., Burbach, M.E., Howard, L.M., Joeckel, R.M., 2010. Nebraska statewide groundwater-level monitoring report 2010.

Li, H.W., Qiao, G., Wu, Y.J., Cao, Y.J., Mi, H., 2017. Water level monitoring on Tibetan lakes based on ICESat and ENVISat data series. Int. Arch. Photogrammetry Remote Sens. Spatial Inform. Sci. - ISPRS Arch. 1529–1533. https://doi.org/10.5194/isprsarchives-XLII-2-W7-1529-2017

Li, J., Heap, A.D., 2008. A review of spatial interpolation methods for environmental scientists.

Lischeid, G., Natkhin, M., Steidl, J., Dietrich, O., Dannowski, R., Merz, C., 2010. Assessing coupling between lakes and layered aquifers in a complex Pleistocene landscape based on water level dynamics. Adv. Water Resour. 33 (11), 1331–1339. https://doi.org/10.1016/j.advwatres.2010.08.002

Liu, D., Wang, Z., Zhang, B., Song, K., Li, X., Li, J., Li, F., Duan, H., 2006. Spatial distribution of soil organic carbon and analysis of related factors in croplands of the black soil region, Northeast China. Agric. Ecosyst. Environ. 113 (1-4), 73–81. https://doi.org/10.1016/j.agee.2005.09.006

Loope, D., Swinehart, J., 2000. Thinking Like a Dune Field: Geologic History in the Nebraska Sand Hills. Gt. Plains Res. A J. Nat. Soc, Sci.

Ma, J., Edmunds, W.M., 2006. Groundwater and lake evolution in the Badain Jaran Desert ecosystem, Inner Mongolia. Hydrogeol. J. 14 (7), 1231–1243. https://doi.org/10.1007/s10040-006-0045-0

Ma, S., Zhou, Y., Gowda, P.H., Dong, J., Zhang, G., Kakani, V.G., Wagle, P., Chen, L., Flynn, K.C., Jiang, W., 2019. Application of the water-related spectral reflectance indices: A review. Ecol. Indic. 98, 68–79. https://doi.org/10.1016/j.ecolind.2018.10.049

McGaughey, R.J., 2009. FUSION/LDV: Software for LIDAR data analysis and visualization. US Dep. Agric. For. Serv. Pacific Northwest Res. Stn, Seattle, WA, USA, p. 123.

McGuire, V.L., 2017. Water-Level and Recoverable Water in Storage Changes, High Plains Aquifer, Predevelopment to 2015 and 2013-15. U.S. Geol. Surv. Sci. Investig. Rep. 2017–5040 14. https://doi.org/10.3133/SIR20175040

Meixner, T., Manning, A.H., Stonestrom, D.A., Allen, D.M., Ajami, H., Blasch, K.W., Brookfield, A.E., Castro, C.L., Clark, J.F., Gochis, D.J., Flint, A.L., Neff, K.L., Niraula, R., Rodell, M., Scanlon, B.R., Singha, K., Walvoord, M.A., 2016. Implications of projected climate change for groundwater recharge in the western United States. J. Hydrol. 534, 124–138. https://doi.org/10.1016/j.jhydrol.2015.12.027

Merz, C., Pekdeger, A., 2011. Climate change-Water and solutes flux-Pleistocene landscape-Water management, ERDE.

Milan, D.J., Heritage, G.L., Large, A.R.G., Entwistle, N.S., 2010. Mapping hydraulic biotopes using terrestrial laser scan data of water surface properties. Earth Surf. Process. Landforms 35 (8), 918–931. https://doi.org/10.1002/esp.v35:810.1002/esp.1948

National Climatic Data Center, N.O. and A.A., 2020. No Title [WWW Document]. Online Clim. Data. URL https://www.ncdc.noaa.gov/cdo-web/datasets (accessed 9.22.20).

Nebraska Department of Natural Resources, 2019. 2019 Nebraska Groundwater Quality Monitoring Report.

Nielsen, K., Stenseng, L., Andersen, O.B., Knudsen, P., 2017. The performance and potentials of the CryoSat-2 SAR and SARIn modes for lake level estimation. Water (Switzerland) 9, 374. https://doi.org/10.3390/w9060374

Ong, J., 2010. Investigation of spatial and temporal processes of lake-aquifer interactions in the Nebraska Sand Hills. Diss. Theses Earth Atmos. Sci. 13, 314.

Paul, J.D., Buytaert, W., Sah, N., 2020. A technical evaluation of lidar-based measurement of river water levels. Water Resour. Res. 56 (4) https://doi.org/10.1029/2019WR026810

Pebesma, E., Graeler, B., 2013. gstat: Spatial and spatio-temporal geostatistical modelling, prediction and simulation. R Packag. version.

Peterson, S.M., Flynn, A.T., Traylor, J.P., 2016. Water Availability and Use Science Program Groundwater-Flow Model of the Northern High Plains Aquifer in Colorado, Kansas, Nebraska, South Dakota, and Wyoming Scientific Investigations Report 2016–5153 Time series of simulated and estimated base flow Grou. Scientific Invest. Report. https://doi.org/10.3133/SIR20165153

Peterson, S.M., Traylor, J.P., Guira, M., 2020. Groundwater Availability of the Northern High Plains Aquifer in Colorado, Kansas, Nebraska, South Dakota, and Wyoming, U. S. Geological Survey. https://doi.org/10.3133/pp1864

Qi, Y., Liu, D., Huang, X., Pu, X., 2019. Topographical mapping of a bare tidal flat outside a mangrove area based on the waterline method and an iterative hydrodynamic model: A Case Study of Yingluo Bay, South China. Mar. Geod. 42 (3), 263–285. https://doi.org/10.1080/01490419.2019.1583617

Riveros-Iregui, D.A., Lenters, J.D., Peake, C.S., Ong, J.B., Healey, N.C., Zlotnik, V.A., 2017. Evaporation from a shallow, saline lake in the Nebraska Sandhills: Energy balance drivers of seasonal and interannual variability. J. Hydrol. 553, 172–187. https://doi.org/10.1016/j.jhydrol.2017.08.002

Rivest, M., Marcotte, D., Pasquier, P., 2008. Hydraulic head field estimation using kriging with an external drift: A way to consider conceptual model information. J. Hydrol. 361 (3-4), 349–361. https://doi.org/10.1016/j.jhydrol.2008.08.006

Roohi, S., Sneeuw, N., Benveniste, J., Dinardo, S., Issawy, E.A., Zhang, G., 2019. Evaluation of CryoSat-2 water level derived from different retracking scenarios over selected inland water bodies. Adv. Sp. Res. 68:2, 947–962. https://doi.org/10.1016/j.asr.2019.06.024

Rossman, N.R., Zlotnik, V.A., Rowe, C.M., 2018. An approach to hydrogeological modeling of a large system of groundwater-fed lakes and wetlands in the Nebraska Sand Hills / Approche par modélisation hydrogéologique d'un vaste système de lacs et de zones humides alimentés par des eaux souterraines dans les Sand Hills du Nebraska, Etats-Unis d'Amérique / Un enfoque para la modelización hidrogeol´ogica de un gran sistema de lagos y humedales alimentados por agua subterr´anea en Nebraska Sand Hills, EE UU / 美国内布拉斯加州Sand Hills地区地下水补给的湖泊和湿地巨大系 统的水文地质模拟方法 / Uma abordagem para modelagem hidrogeológica de um amplo sistema de lagos e zonas húmidas alimentados por águas subterrâneas em Nebraska Sand Hills, EUA. USA. Hydrogeol. J. 26 (3), 881–897. https://doi.org/10.1007/s10040-017-1691-0

Rossman, N.R., Zlotnik, V.A., Rowe, C.M., Szilagyi, J., 2014. Vadose zone lag time and potential 21st century climate change effects on spatially distributed groundwater recharge in the semi-arid Nebraska Sand Hills. J. Hydrol. 519, 656–669. https://doi.org/10.1016/j.jhydrol.2014.07.057

Ryan, J.C., Smith, L.C., Cooley, S.W., Pitcher, L.H., Pavelsky, T.M., 2020. Global Characterization of Inland Water Reservoirs Using ICESat-2 Altimetry and Climate Reanalysis. Geophys. Res. Lett. 47 (17) https://doi.org/10.1029/2020GL088543

Sacks, L.A., Herman, J.S., Konikow, L.F., Vela, A.L., 1992. Seasonal dynamics of groundwater-lake interactions at Doñana National Park. Spain. J. Hydrol. 136 (1-4), 123–154. https://doi.org/10.1016/0022-1694(92)90008-J

Scanlon, B.R., Faunt, C.C., Longuevergne, L., Reedy, R.C., Alley, W.M., McGuire, V.L., McMahon, P.B., 2012. Groundwater depletion and sustainability of irrigation in the US High Plains and Central Valley. Proc. Natl. Acad. Sci. U. S. A. 109 (24), 9320–9325. https://doi.org/10.1073/pnas.1200311109

Scanlon, B.R., Keese, K.E., Flint, A.L., Flint, L.E., Gaye, C.B., Edmunds, W.M., Simmers, I., 2006. Global synthesis of groundwater recharge in semiarid and arid regions. Hydrol. Process. 20 (15), 3335–3370. https://doi.org/10.1002/(ISSN)1099-108510.1002/hyp.v20:1510.1002/hyp.6335

Shi, T., Xu, H., 2019. Derivation of Tasseled Cap Transformation Coefficients for Sentinel-2 MSI At-Sensor Reflectance Data. IEEE J. Sel. Top. Appl. Earth Obs. Remote Sens. 12 (10), 4038–4048. https://doi.org/10.1109/JSTARS.460944310.1109/JSTARS.2019.2938388

Shrestha, N., Mittelstet, A.R., Gilmore, T.E., Zlotnik, V.A., Neale, C.M.U., 2021. Effects of drought on groundwater-fed lake areas in the Nebraska Sand Hills. J. Hydrol. Reg, Stud. In Revision.

Singh, A., Mishra, S., Ruskauff, G., 2010. Model Averaging Techniques for Quantifying Conceptual Model Uncertainty. Ground Water 48, 701–715. https://doi.org/10.1111/j.1745-6584.2009.00642.x

Smith, H.T.U., 1965. Dune morphology and chronology in central and Western Nebraska. J. Geol. 73 (4), 557–578. https://doi.org/10.1086/627093

Speldrich, B., Gerla, P., Tschann, E., 2021. Characterizing groundwater interaction with lakes and wetlands using GIS modeling and natural water quality measurements. Water (Switzerland) 13, 983. https://doi.org/10.3390/w13070983

Stehman, S.V., 1997. Selecting and interpreting measures of thematic classification accuracy. Remote Sens. Environ. 62 (1), 77–89. https://doi.org/10.1016/S0034-4257(97)00083-7

Strassberg, G., Scanlon, B.R., Chambers, D., 2009. Evaluation of groundwater storage monitoring with the GRACE satellite: Case study of the High Plains aquifer, central United States. Water Resour. Res. 45 (5) https://doi.org/10.1029/2008WR006892

Suttie, J.M., Reynolds, S.G., Batello, C., 2005. Grasslands of the World. Food & Agriculture Org.

Sweeney, M.R., Loope, D.B., 2001. Holocene dune-sourced alluvial fans in the Nebraska Sand Hills. Geomorphology 38 (1-2), 31–46. https://doi.org/10.1016/S0169-555X(00)00067-2

Taylor, R.G., Scanlon, B., Döll, P., Rodell, M., Van Beek, R., Wada, Y., Longuevergne, L., Leblanc, M., Famiglietti, J.S., Edmunds, M., Konikow, L., Green, T.R., Chen, J., Taniguchi, M., Bierkens, M.F.P., Macdonald, A., Fan, Y., Maxwell, R.M., Yechieli, Y., Gurdak, J.J., Allen, D.M., Shamsudduha, M., Hiscock, K., Yeh, P.J.F., Holman, I.,

Treidel, H., 2013. Ground water and climate change. Nat. Clim. Chang. https://doi.org/10.1038/nclimate1744

Theodoridou, P.G., Varouchakis, E.A., Karatzas, G.P., 2017. Spatial analysis of groundwater levels using Fuzzy Logic and geostatistical tools. J. Hydrol. 555, 242–252. https://doi.org/10.1016/j.jhydrol.2017.10.027

Tian, S., Zhang, X., Tian, J., Sun, Q., 2016. Random Forest Classification of Wetland Landcovers from Multi-Sensor Data in the Arid Region of Xinjiang. China. Remote Sens. 8, 954. https://doi.org/10.3390/rs8110954

Tonkin, M.J., Larson, S.P., 2002. Kriging Water Levels with a Regional-Linear and Point- Logarithmic Drift. Ground Water 40 (2), 185–193. https://doi.org/10.1111/gwat.2002.40.issue-210.1111/j.1745-6584.2002.tb02503.x

Turner, J.V., Townley, L.R., 2006. Determination of groundwater flow-through regimes of shallow lakes and wetlands from numerical analysis of stable isotope and chloride tracer distribution patterns, in. J. Hydrol. Elsevier 320 (3-4), 451–483. https://doi.org/10.1016/j.jhydrol.2005.07.050

Tweed, S., Leblanc, M., Cartwright, I., 2009. Groundwater–surface water interaction and the impact of a multi-year drought on lakes conditions in South-East Australia. J. Hydrol. 379 (1-2), 41–53. https://doi.org/10.1016/j.jhydrol.2009.09.043

Varouchakis, E.A., Hristopulos, D.T., 2013. Comparison of stochastic and deterministic methods for mapping groundwater level spatial variability in sparsely monitored basins. Environ. Monit. Assess. 185 (1), 1–19. https://doi.org/10.1007/s10661-012-2527-y

Varouchakis, E.A., Kolosionis, K., Karatzas, G.P., 2016. Spatial variability estimation and risk assessment of the aquifer level at sparsely gauged basins using geostatistical methodologies. Earth Sci. Informatics 9 (4), 437–448. https://doi.org/10.1007/s12145-016-0265-3

Verpoorter, C., Kutser, T., Tranvik, L., 2012. Automated mapping of water bodies using Landsat multispectral data. Limnol. Oceanogr. Methods 10 (12), 1037–1050. https://doi.org/10.4319/lom.2012.10.1037

Wang, C., Jia, M., Chen, N., Wang, W., 2018. Long-Term Surface Water Dynamics Analysis Based on Landsat Imagery and the Google Earth Engine Platform: A Case Study in the Middle Yangtze River Basin. Remote Sens. 10, 1635. https://doi.org/10.3390/rs10101635

Wang, Y., Li, Z., Zeng, C., Xia, G.-S., Shen, H., 2020. An Urban Water Extraction Method Combining Deep Learning and Google Earth Engine. IEEE J. Sel. Top. Appl. Earth Obs. Remote Sens. 13, 769–782. https://doi.org/10.1109/JSTARS.460944310.1109/JSTARS.2020.2971783

Winter, T.C., 1999. Relation of streams, lakes, and wetlands to groundwater flow systems. Hydrogeol. J. 7 (1), 28–45. https://doi.org/10.1007/s100400050178

Winter, T.C., 1986. Effect of ground-water recharge on configuration of the water table beneath sand dunes and on seepage in lakes in the sandhills of Nebraska, U.S.A. J. Hydrol. 86 (3-4), 221–237. https://doi.org/10.1016/0022-1694(86)90166-6

Wolock, D.M., Price, C.V., 1994. Effects of digital elevation model map scale and data resolution on a topography-based watershed model. Water Resour. Res. 30 (11), 3041–3052. https://doi.org/10.1029/94WR01971

Young, A., Burbach, M., Howard, L., Waszgis, M., Lackey, S., Joeckel, R.M., 2019. Nebraska Statewide Groundwater-Level Monitoring Report 2018. Conserv. Surv, Div.

Yuan, C., Gong, P., Bai, Y., 2020. Performance Assessment of ICESat-2 Laser Altimeter Data for Water-Level Measurement over Lakes and Reservoirs in China. Remote Sens. 12, 770. https://doi.org/10.3390/rs12050770

Yue, H., Liu, Y., 2019. Variations in the lake area, water level, and water volume of Hongjiannao Lake during 1986–2018 based on Landsat and ASTER GDEM data. Environ. Monit. Assess. 191, 1–25. https://doi.org/10.1007/s10661-019-7715-6

Zhang, C., Su, H., Li, T., Liu, W., Mitsova, D., Nagarajan, S., Teegavarapu, R., Xie, Z., Bloetscher, F., Yong, Y., 2020. Modeling and Mapping High Water Table for a Coastal Region in Florida using Lidar DEM Data. Groundwater 59:2, 190–198. https://doi.org/10.1111/gwat.13041

Zhang, G., Chen, W., Xie, H., 2019. Tibetan Plateau's Lake Level and Volume Changes From NASA's ICESat/ICESat-2 and Landsat Missions. Geophys. Res. Lett. 46 (22), 13107–13118. https://doi.org/10.1029/2019GL085032

Zhang, G., Yao, T., Shum, C.K., Yi, S., Yang, K., Xie, H., Feng, W., Bolch, T., Wang, L., Behrangi, A., Zhang, H., Wang, W., Xiang, Y., Yu, J., 2017. Lake volume and groundwater storage variations in Tibetan Plateau's endorheic basin. Geophys. Res. Lett. 44 (11), 5550–5560. https://doi.org/10.1002/grl.v44.1110.1002/2017GL073773

Zhuang, Y., Chen, C., 2018. A Method for water body extraction based on the tasselled cap transformation from remote sensing images. In: in: 5th International Workshop on Earth Observation and Remote Sensing Applications, EORSA 2018 - Proceedings. Institute of Electrical and Electronics Engineers Inc. https://doi.org/10.1109/EORSA.2018.8598605

Zlotnik, V.A., Olaguera, F., Ong, J.B., 2009. An approach to assessment of flow regimes of groundwater-dominated lakes in arid environments. J. Hydrol. 371 (1-4), 22–30. https://doi.org/10.1016/j.jhydrol.2009.03.012

Zou, C., Twidwell, D., Bielski, C., Fogarty, D., Mittelstet, A., Starks, P., Will, R., Zhong, Y., Acharya, B., 2018. Impact of Eastern Redcedar Proliferation on Water Resources in the Great Plains USA—Current State of Knowledge. Water 10, 1768. https://doi.org/10.3390/w10121768